Ultrafast 2D IR microscopy

Carlos R. Baiz, Denise Schach, and Andrei Tokmakoff*

Department of Chemistry, James Franck Institute and Institute for Biophysical Dynamics, The University of Chicago, 929 E 57th St, Chicago, IL USA

tokmakoff@uchicago.edu

Abstract: We describe a microscope for measuring two-dimensional infrared (2D IR) spectra of heterogeneous samples with μm-scale spatial resolution, sub-picosecond time resolution, and the molecular structure information of 2D IR, enabling the measurement of vibrational dynamics through correlations in frequency, time, and space. The setup is based on a fully collinear "one beam" geometry in which all pulses propagate along the same optics. Polarization, chopping, and phase cycling are used to isolate the 2D IR signals of interest. In addition, we demonstrate the use of vibrational lifetime as a contrast agent for imaging microscopic variations in molecular environments.

OCIS codes: (300.0300) Spectroscopy; (300.6530) Spectroscopy, ultrafast; (300.6340) Spectroscopy, infrared; (320.5540) Pulse shaping; (110.0180) Microscopy; (180.4315) Nonlinear microscopy.

References and links

1. J. Manor, P. Mukherjee, Y. S. Lin, H. Leonov, J. L. Skinner, M. T. Zanni, and I. T. Arkin, "Gating mechanism of the influenza A M2 channel revealed by 1D and 2D IR spectroscopies," Structure **17**(2), 247–254 (2009).
2. A. Remorino and R. M. Hochstrasser, "Three-dimensional structures by two-dimensional vibrational spectroscopy," Acc. Chem. Res. **45**(11), 1896–1905 (2012).
3. M. D. Fayer, "Water in a crowd," Physiology **26**(6), 381–392 (2011).
4. A. A. Bakulin, C. Liang, T. la Cour Jansen, D. A. Wiersma, H. J. Bakker, and M. S. Pshenichnikov, "Hydrophobic solvation: a 2D IR spectroscopic inquest," Acc. Chem. Res. **42**(9), 1229–1238 (2009).
5. D. G. Kuroda, J. D. Bauman, J. R. Challa, D. Patel, T. Troxler, K. Das, E. Arnold, and R. M. Hochstrasser, "Snapshot of the equilibrium dynamics of a drug bound to HIV-1 reverse transcriptase," Nat. Chem. **5**(3), 174–181 (2013).
6. H. S. Chung, M. Khalil, A. W. Smith, Z. Ganim, and A. Tokmakoff, "Conformational changes during the nanosecond-to-millisecond unfolding of ubiquitin," Proc. Natl. Acad. Sci. U.S.A. **102**(3), 612–617 (2005).
7. M. S. Lynch, K. M. Slenkamp, and M. Khalil, "Communication: Probing non-equilibrium vibrational relaxation pathways of highly excited C≡N stretching modes following ultrafast back-electron transfer," J. Chem. Phys. **136**(24), 241101 (2012).
8. C. R. Baiz, R. McCanne, and K. J. Kubarych, "Structurally selective geminate rebinding dynamics of solvent-caged radicals studied with nonequilibrium infrared echo spectroscopy," J. Am. Chem. Soc. **131**(38), 13590–13591 (2009).
9. L. W. Barbour, M. Hegadorn, and J. B. Asbury, "Watching electrons move in real time: ultrafast infrared spectroscopy of a polymer blend photovoltaic material," J. Am. Chem. Soc. **129**(51), 15884–15894 (2007).
10. H. Chen, X. Wen, J. Li, and J. Zheng, "Molecular distances determined with resonant vibrational energy transfers," J. Phys. Chem. A **118**(13), 2463–2469 (2014).
11. C. S. Peng, K. C. Jones, and A. Tokmakoff, "Anharmonic vibrational modes of nucleic acid bases revealed by 2D IR spectroscopy," J. Am. Chem. Soc. **133**(39), 15650–15660 (2011).
12. M. Cho, "Coherent two-dimensional optical spectroscopy," Chem. Rev. **108**(4), 1331–1418 (2008).
13. C. S. Peng, C. R. Baiz, and A. Tokmakoff, "Direct observation of ground-state lactam-lactim tautomerization using temperature-jump transient 2D IR spectroscopy," Proc. Natl. Acad. Sci. U.S.A. **110**(23), 9243–9248 (2013).
14. C. R. Baiz, C. S. Peng, M. E. Reppert, K. C. Jones, and A. Tokmakoff, "Coherent two-dimensional infrared spectroscopy: quantitative analysis of protein secondary structure in solution," Analyst **137**(8), 1793–1799 (2012).
15. R. Salzer and H. W. Siesler, *Infrared and Raman Spectroscopic Imaging* (Wiley-VCH, 2009).
16. D. I. Ellis and R. Goodacre, "Metabolic fingerprinting in disease diagnosis: biomedical applications of infrared and Raman spectroscopy," Analyst **131**(8), 875–885 (2006).

#213680 - $15.00 USD Received 13 Jun 2014; revised 16 Jul 2014; accepted 16 Jul 2014; published 25 Jul 2014

17. M. C. Martin, C. Dabat-Blondeau, M. Unger, J. Sedlmair, D. Y. Parkinson, H. A. Bechtel, B. Illman, J. M. Castro, M. Keiluweit, D. Buschke, B. Ogle, M. J. Nasse, and C. J. Hirschmugl, "3D spectral imaging with synchrotron Fourier transform infrared spectro-microtomography," Nat. Methods **10**(9), 861–864 (2013).
18. A. Remorino, I. V. Korendovych, Y. B. Wu, W. F. DeGrado, and R. M. Hochstrasser, "Residue-specific vibrational echoes yield 3D structures of a transmembrane helix dimer," Science **332**(6034), 1206–1209 (2011).
19. P. Tian, D. Keusters, Y. Suzaki, and W. S. Warren, "Femtosecond phase-coherent two-dimensional spectroscopy," Science **300**(5625), 1553–1555 (2003).
20. W. Wagner, C. Li, J. Semmlow, and W. Warren, "Rapid phase-cycled two-dimensional optical spectroscopy in fluorescence and transmission mode," Opt. Express **13**(10), 3697–3706 (2005).
21. B. J. Davis, P. S. Carney, and R. Bhargava, "Theory of midinfrared absorption microspectroscopy: I. Homogeneous samples," Anal. Chem. **82**(9), 3474–3486 (2010).
22. S. H. Shim and M. T. Zanni, "How to turn your pump-probe instrument into a multidimensional spectrometer: 2D IR and Vis spectroscopies via pulse shaping," Phys. Chem. Chem. Phys. **11**(5), 748–761 (2009).
23. P. Hamm and M. T. Zanni, *Concepts and Methods of 2D Infrared Spectroscopy* (Cambridge University, 2011).
24. G. Cinque, M. D. Frogley, and R. Bartolini, "Far-IR/THz spectral characterization of the coherent synchrotron radiation emission at diamond IR beamline B22," Rendiconti Lincei **22**(1), 33–47 (2011).
25. C. R. Baiz, P. L. McRobbie, N. K. Preketes, K. J. Kubarych, and E. Geva, "Two-dimensional infrared spectroscopy of dimanganese decacarbonyl and its photoproducts: an ab initio study," J. Phys. Chem. A **113**(35), 9617–9623 (2009).
26. C. R. Baiz, K. J. Kubarych, E. Geva, and E. L. Sibert 3rd, "Local-mode approach to modeling multidimensional infrared spectra of metal carbonyls," J. Phys. Chem. A **115**(21), 5354–5363 (2011).
27. L. Wei, Y. Yu, Y. H. Shen, M. C. Wang, and W. Min, "Vibrational imaging of newly synthesized proteins in live cells by stimulated Raman scattering microscopy," Proc. Natl. Acad. Sci. U.S.A. **110**(28), 11226–11231 (2013).
28. K. König, "Multiphoton microscopy in life sciences," J. Microsc. **200**(2), 83–104 (2000).
29. J. A. Myers, K. L. Lewis, P. F. Tekavec, and J. P. Ogilvie, "Two-color two-dimensional Fourier transform electronic spectroscopy with a pulse-shaper," Opt. Express **16**(22), 17420–17428 (2008).
30. A. Zoubir, *Raman Imaging: Techniques and Applications* (Springer, 2012).
31. D. Fu, F. K. Lu, X. Zhang, C. Freudiger, D. R. Pernik, G. Holtom, and X. S. Xie, "Quantitative chemical imaging with multiplex stimulated Raman scattering microscopy," J. Am. Chem. Soc. **134**(8), 3623–3626 (2012).
32. H. Frostig, O. Katz, A. Natan, and Y. Silberberg, "Single-pulse stimulated Raman scattering spectroscopy," Opt. Lett. **36**(7), 1248–1250 (2011).
33. J. P. Ogilvie, E. Beaurepaire, A. Alexandrou, and M. Joffre, "Fourier-transform coherent anti-Stokes Raman scattering microscopy," Opt. Lett. **31**(4), 480–482 (2006).

1. Introduction

Chemical and structural specificity make infrared spectroscopy a powerful experimental technique in virtually all molecular sciences, from materials chemistry and nanoscience to molecular biology and biomedical engineering. During the past 15 years, ultrafast time-resolved IR spectroscopy—two-dimensional infrared (2D IR) spectroscopy in particular—has experienced tremendous advances in both new methods and applications. For example, 2D IR has found applications in the study of processes such as membrane protein dynamics [1, 2], water dynamics and confinement [3, 4], protein–drug interactions [5], fast protein folding [6], transient photochemical dynamics [7, 8], or charge separation in organic photovoltaic materials [9]. Indeed, 2D IR spectra offer a wealth of molecular information, including: *1*. molecular structure, as observed in the off-diagonal peaks that arise from vibrational coupling or relative dipole orientations that are extracted from polarization-dependent spectra [10, 11]; *2*. molecular dynamics, which are obtained from vibrational dynamics measurements such as spectral diffusion, orientational relaxation rate, and vibrational lifetime; *3*. rates of chemical exchange between different species [12]; and *4*. 2D IR has a unique ability to spectrally disentangle complex mixtures, for instance isomers or protein structures [13, 14].

In parallel, developments in optical imaging and microscopy have led to many revolutionary advances in nearly all areas of biology, medicine, and materials science and engineering. Spatial resolution and image contrast are obtained through a variety of methods, but the vast majority of optical microscopy measures microscopic spatial variation in the optical properties of a sample (absorption, emission, dispersion, or scattering). Such measurements have the advantage of noninvasive imaging with submicron resolution in space, but the measured chemical information is typically limited to concentration variations

#213680 - $15.00 USD Received 13 Jun 2014; revised 16 Jul 2014; accepted 16 Jul 2014; published 25 Jul 2014

for specific chromophores in space. Additionally, time scales for spatially resolved dynamics are commonly limited by the detection electronics. Vibrational imaging, in the form of IR or Raman, takes advantage of the chemical specificity of molecular vibrations to measure the distribution of individual species based on their spectroscopic signatures in order to create a chemically selective map without the need for labels or stains [15] and significant efforts have been directed toward imaging molecular vibrations for biological and clinical applications [16, 17].

The motivation behind the work presented here is to extend the capabilities of IR microscopy by incorporating ultrafast nonlinear IR spectroscopy in order to measure spatially resolved information on molecular structure and dynamics not available by traditional methods [12]. While the direct spatial resolution of IR microscopy is limited by diffraction to 2–10 μm, 2D IR spectroscopy can indirectly reveal molecular structures to sub-Ångstrom precision [18]. Similarly, while IR detectors are slow, the experimental time resolution, dictated by the optical delays between femtosecond IR pulses, is below a picosecond. Finally, while microscopy separates molecular ensembles based on their spatial distribution, 2D IR spectroscopy separates chemical ensembles based on vibrational frequency, where off-diagonal peaks report on frequency correlations and vibrational coupling within ensembles on sub-picosecond time scales. This is particularly useful for dissecting complex molecular mixtures. These new tools would provide unique capabilities in studies of systems with complex behavior over multiple spectral and temporal scales.

The key enabling breakthrough is an optical implementation where all three pulses and the signal for the 2D IR experiment propagate fully collinearly [Fig. 1], analogous to previous implementations developed for 2D electronic spectroscopy [19, 20]. To date, 2D IR spectroscopy has been implemented primarily with beams crossed at the sample to assist in separating the coherent wavevector-matched signal from the transmitted input pulses (I_S/I_{Input}~10^{-7}–10^{-9}). A collinear experiment is complicated by the task of isolating the 2D IR signal from the multiple interferences between transmitted fields. However, the "one beam" arrangement facilitates the optical alignment, allows focusing with high numerical aperture, and enables new implementations of 2D IR spectroscopy. Here we describe the isolation of the 2D IR signals in collinear experiments using a combination of phase cycling, polarization control, and mechanical chopping, and our first steps in transmission and transflection (transmission–reflection) [21] microscopy near the diffraction limit.

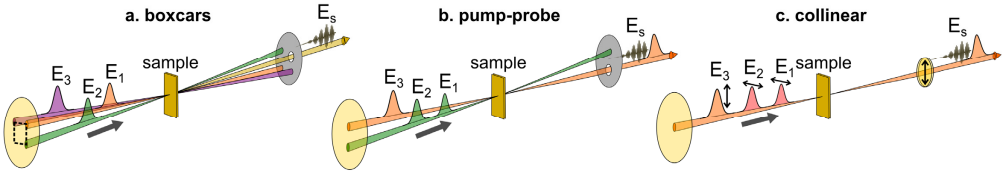

Fig. 1. Optical geometries used for 2D IR spectroscopy. (a) Boxcars geometry, where all three incoming pulses and the signal propagate in different directions. (b) Pump–probe geometry, the two pumps (E_1 and E_2) travel collinearly with each other but not with the probe (E_3). In both geometries the signal is isolated by a spatial mask. (c) Collinear geometry used for IR microscopy. In this case the pump pulses are blocked by a wire-grid polarizer.

2. Methods

2.1 Optical layout

The experimental setup for collinear 2D IR spectroscopy in a microscope is shown in Fig. 2. Mid-infrared pulses (100 fs) centered at 5 μm (2000 cm^{-1}) are generated in $AgGaS_2$ by difference frequency generation of the signal and idler outputs of an OPA (TOPAS-C, Light Conversion) pumped by a 1 kHz amplified Ti:Sapphire laser (Libra, Coherent Inc). The probe pulse is split off by the weak reflection from an uncoated, wedged CaF_2 window and sent

#213680 - $15.00 USD Received 13 Jun 2014; revised 16 Jul 2014; accepted 16 Jul 2014; published 25 Jul 2014

through an optical delay line with a mechanical delay stage (ANT-95, Aerotech Inc). The main beam is routed into a germanium acousto-optic pulse shaper (QuickShape, PhaseTech Spectroscopy Inc.) in order to generate the time-delayed pump pulses [22]. The probe polarization is rotated by 90° with a λ/2 plate (Karl Lambrecht Corp.), and the probe beam is reoverlapped with the pump pulses in a wire-grid polarizer (Specac Limited) that transmits the pump pulses and reflects the probe. Dispersion of the pump pulses caused by the polarizer is precompensated for with the pulse shaper. From this point all of the pulses travel fully collinearly along common optics, through the microscope and into the detector.

The beam is routed into a mid-IR microscope (Hyperion 2000, Bruker Optics), equipped with a reflective Schwarzchild-type objective and matched condenser (15 × , NA = 0.4). The microscope can operate in transmission or reflection mode. For reflection mode, a beamsplitter is positioned immediately before the objective and the IR is routed in and out through the objective. For transmission mode, the IR is focused into the sample by the condenser and collected through the objective. An analyzing polarizer is placed immediately after the objective to block the pump pulses and transmit the probe and signal. The output of the microscope is collimated by a 10-cm focal length CaF_2 lens and routed into a spectrometer equipped with a 150 lines/mm grating, which disperses the spectrum onto a 64-pixel mercury–cadmium–telluride (MCT) array detector (Infrared Systems Development). A third polarizer (analyzer) with the same orientation as the second polarizer (i.e., perpendicular to the first polarizer) is placed in front of the spectrometer, which serves to reduce residual pump light by about 50%. Given the polarization scheme used here, spectra are collected in the crossed polarization (XXYY) geometry exclusively.

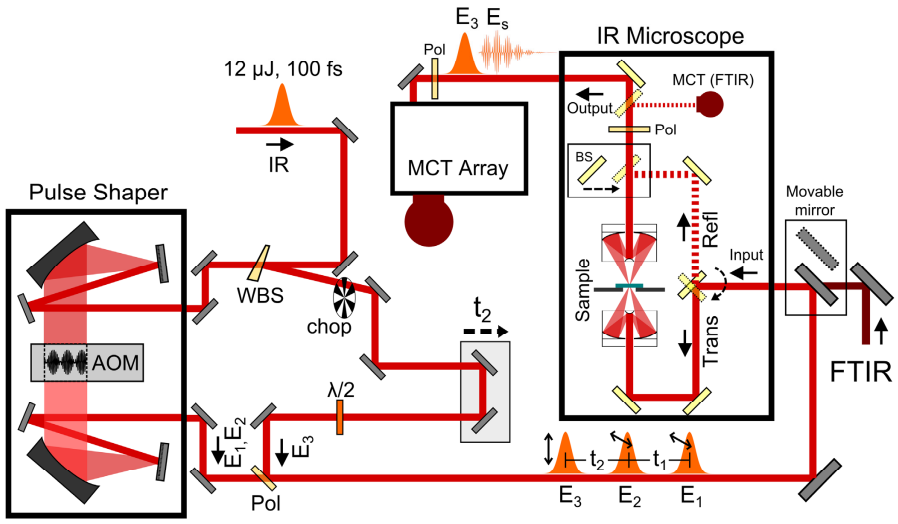

Fig. 2. Optical layout of the ultrafast mid-IR microscopy setup. The pulses are generated by an OPA-DFG setup (not shown), part of the light is split by a wedged beamsplitter (WBS) and travels along the variable-delay probe (E_3) path. The pulse shaper generates the pump pulses (E_1 and E_2), which are combined with a probe at a wire-grid polarizer (Pol) and routed into the microscope. The microscope can be automatically configured to record spectra in transmission or reflection modes. At the output of the microscope a motorized mirror switches between a single channel MCT detector for FTIR measurements and a grating-based spectrometer equipped with an MCT array for 2D IR spectroscopy.

In order to collect a 2D IR spectrum, the delay between the pump pulses (t_1) is scanned in 45 fs steps to a maximum delay of 5.985 ps, producing a spectral resolution along the excitation axis of 5.6 cm^{-1}. The resolution along the probe (detection) axis, dictated by the grating and pixel size of the MCT array, is 2.4 cm^{-1}. An eight-frame phase cycle, described in

#213680 - $15.00 USD Received 13 Jun 2014; revised 16 Jul 2014; accepted 16 Jul 2014; published 25 Jul 2014

Table 1, is applied at each t_1 delay. The next section provides a brief description of the time delays scanned and the pulse-cycling scheme used to isolate the signals of interest.

In addition, the microscope is attached to a commercial FTIR spectrometer (Vertex 70, Bruker Optics) for linear FTIR absorption, reflectance microscopy, and visible optical imaging. For FTIR measurements, a movable mirror routes the output of the microscope into a single-channel MCT detector. Similarly, a second mirror selects between the FTIR and 2D IR input beams.

2.2 Isolating nonlinear signals

In general, third-order nonlinear signals are generated by the interaction of three input fields E_j with the sample. The interaction is described by the material response function R, which for 2D IR experiments is composed of the rephasing and nonrephasing response functions, $R^{(R)}$ and $R^{(NR)}$. The resulting third-order polarization acts to radiate a signal field E_{2DIR} into a phase-matched direction dictated by the wavevectors of the incoming pulses. From a molecular perspective, the first pulse induces a vibrational coherence between the ground and lowest excited eigenstates of the system. The time delay between the first and second pulses is referred to as the first coherence time (t_1), and Fourier transformation with respect to this delay produces the excitation frequency. The second pulse locks the coherence into either a ground- or an excited-state population and the delay following the second pulse (t_2) is referred to as waiting, or population time. Finally, the third pulse induces a second coherence either between ground and first excited state or between the first and second excited states. The ground and excited-state coherences are phase shifted by π with respect to the probe pulse, giving rise to the positive/negative peak pairs observed along the detection axis in the 2D IR spectrum.

The input pulses can be written in terms of their field envelope ε_i, wavevector $\vec{k}_i$, carrier frequency ω_i and phase ϕ_i,

$$\vec{E}_j(t) = \vec{\varepsilon}_j(t) e^{i\vec{k}_j \cdot \vec{r} - i\omega_j t + \phi_j}, \tag{1}$$

where j = 1,2,3. We refer to the first two pulses, with wavevectors $\vec{k}_1$ and $\vec{k}_2$ as pumps and the third pulse $\vec{k}_3$ as a probe. The phase-matching conditions for rephasing and nonrephasing signals are $\vec{k}_R = -\vec{k}_1 + \vec{k}_2 + \vec{k}_3$ and $\vec{k}_{NR} = +\vec{k}_1 - \vec{k}_2 + \vec{k}_3$, respectively. Then, neglecting the frequency arguments, the time-domain signal field in the impulsive limit can be written as [23]:

$$\begin{aligned} E_{2DIR}(t_1,t_2,t_3) \propto \quad & \mathrm{R}^{(R)}(t_1,t_2,t_3) e^{i(-\vec{k}_1+\vec{k}_2+\vec{k}_3)\cdot\vec{r}} e^{i(-\phi_1+\phi_2+\phi_3)} \\ & + \mathrm{R}^{(NR)}(t_1,t_2,t_3) e^{i(+\vec{k}_1-\vec{k}_2+\vec{k}_3)\cdot\vec{r}} e^{i(+\phi_1-\phi_2+\phi_3)} \end{aligned} \tag{2}$$

The spectral phase and amplitude of the emitted signal is measured by the interference with a reference pulse, or local oscillator (LO). In our collinear geometry $\vec{k}_1 = \vec{k}_2 = \vec{k}_3 = \vec{k}_{LO}$, so that

$$\begin{aligned} S_{2DIR}(\phi_1,\phi_2,\phi_3,\phi_{LO}) &= \mathrm{Re}[E_{2DIR} E_{LO}^*] \\ &\propto \mathrm{Re}\left(\mathrm{R}^{(R)} e^{i(-\phi_1+\phi_2+\phi_3-\phi_{LO})} + \mathrm{R}^{(NR)} e^{i(+\phi_1-\phi_2+\phi_3-\phi_{LO})}\right) \end{aligned} \tag{3}$$

In the pump–probe and collinear geometries, the transmitted probe pulse also serves as the LO. Thus $\phi_3 = \phi_{LO}$, and the 2D IR signal phase depends only on the relative phase between the first two pulses $\phi_1 - \phi_2$. In the present implementation, 2D IR spectra are measured in the mixed time–frequency domain. The excitation axis is measured in the time domain by

#213680 - $15.00 USD Received 13 Jun 2014; revised 16 Jul 2014; accepted 16 Jul 2014; published 25 Jul 2014

scanning t_1, the envelope delay between the pump pulses using varying carrier phases ϕ_1 and ϕ_2. The detection axis (ω_3) is measured directly in the frequency domain by spectrally dispersing the signal and transmitted probe in a grating spectrometer. Fourier transformation along t_1 produces the pump frequency axis (ω_1). The waiting time (t_2) is typically fixed at a specific delay, so that the final 2D IR spectrum is represented as a 2D plot of ω_1 versus ω_3 for a specific value of t_2.

Although polarizers block the majority of the pump light after the sample, the high energy of the pulses combined with the relatively low contrast ratio of wire-grid polarizers causes a significant amount of pump energy to leak through to the detector. The detector will observe all transmitted fields and a variety of nonlinear signals that radiate into the same phase-matched direction among which is the 2D IR signal of interest

$$S_{TOT} \propto \left| E_1 + E_2 + E_3 + E_{other} + E_{2DIR} \right|^2 \tag{4}$$

Here E_3 is the strongest field, followed by E_1 and E_2, and the nonlinear signals are the weakest. In the following paragraphs we describe the approach to isolate E_{2DIR}, or more formally, the interference term in Eq. (3). This is accomplished with a combination of *1.* Fourier filtering, *2.* phase cycling, and *3.* chopping. Fourier filtering refers to isolating time-domain signals that oscillate at frequencies within the pulse bandwidth. Since the measurement is carried out by scanning E_1 in time and the signal of interest oscillates at frequencies $\approx\omega_1$, a numerical Fourier transform along t_1 suppresses signals that do not oscillate with respect to this delay.

Table 1. Phase-cycling scheme used for removing unwanted field interferences and isolating the nonlinear signals of interest.

	Phase						
	Input Fields			Detected			
Frame	φ_1	φ_2	φ_3	E_1E_2	E_1E_3	E_2E_3	S_{2DIR}
A	0	0	0	0	0	0	0
B	0	π	0	π	0	π	π[a]
C	π	0	0	π	π	0	π[a]
D	π	π	0	0	π	π	0
E	0	0	—	0	—	—	—
F	0	π	—	π	—	—	—
G	π	0	—	π	—	—	—
H	π	π	—	0	—	—	—

Signal I (chopper phase: k3, open): (B + C)-(A + D) = $4S_{2DIR} + 4E_1E_2$
Signal II (chopper phase: k3, blocked): (F + G)-(E + H) = $4E_1E_2$
Signal I – Signal II = $4S_{2DIR}$

0 and π refer to the carrier phase of the field generated by the pulse shaper, and the resulting phase of an interference term or 2D IR signal. Signals that are in phase (0) or out of phase (π) cancel out when the two frames are subtracted or added. The dashes (—) refer to the chopper phase, indicating that the probe field and the corresponding output signals are blocked. [a] Strictly speaking, the phase is either + π or -π as dictated by the response functions [see Eq. (3)].

Linear interference terms: Next, to remove unwanted linear interference terms between transmitted fields that oscillate at $\approx\omega_1$ and isolate the 2D IR signal, we exploit the unique capability of the pulse shaper to phase cycle the pump pulses. Shifting the phase of the carrier wave for E_1 or E_2 by π inverts the 2D IR signal, allowing for shot-to-shot difference detection that removes unchanged linear interference terms. Since the interference between E_1 and E_2 has the same phase dependence as the 2D IR signal, it cannot be removed by phase cycling the pumps alone. This term is therefore removed by mechanically chopping the probe. Table 1 summarizes the phase of different interference signals for a given set of input phases, and the differential detection scheme used to remove the unwanted pulse interferences using an eight-frame phase cycle.

#213680 - $15.00 USD Received 13 Jun 2014; revised 16 Jul 2014; accepted 16 Jul 2014; published 25 Jul 2014

Other nonlinear signals (E_{other}): In addition to the 2D IR signal [Eq. (2)] and linear interference terms (Table 1), it is important to consider additional wavevector-matched nonlinear signals emitted in the direction of the probe ($\vec{k}_{other} = \vec{k}_3$) [see Eq. (4)]. The boxcars and pump–probe geometries [Fig. 1] take advantage of specific beam configurations to block nonlinear signals that are not wavevector-matched using a spatial mask after the sample. However, with a fully collinear beam propagation there are additional signals propagating in the direction of the probe ($\vec{k}_S$). Out of 60 total possible wavevector-matched third-order signals that arise from the interaction of three pulses with the sample we only consider terms that satisfy the following criteria: *1. Pulse ordering:* Interactions with the pulses must be sequential (i.e., $\pm\vec{k}_1 \pm \vec{k}_2 \pm \vec{k}_3$). This is because the pulses are separated in time, except at $t_1 = 0$. *2. Weak probe:* Since the signal scales linearly with the probe field, and the pumps are much stronger than the probe, multiple interactions with the same pulse can occur with the pumps only. *3. Polarization:* Only signals that are allowed in the crossed polarization geometry of this instrument (i.e., XXYY tensor elements) are measured. The eight signals that meet all three criteria are listed in Table 2. Two of these signals correspond to the rephasing and nonrephasing contributions, and two correspond to transient absorption (pump–probe) signals with either of the two pump pulses that are removed in Fourier filtering. Four double-quantum coherence signals also appear in the collinear geometry. Two of these signals will oscillate along t_2 at twice the fundamental frequency of the molecular vibration, but are not expected to oscillate along t_1, and are therefore not expected to contribute to the measured Fourier transform 2D IR spectra that oscillate near the carrier frequency.

Table 2. Wavevector matched third-order nonlinear signals observed in the collinear geometry.

Polarization				
X	**X**	**Y**	**Y**	**Signal**
$-k_1$	$+k_2$	$+k_3$	k_s	Rephasing
$+k_1$	$-k_2$	$+k_3$	k_s	Nonrephasing
$+k_1$	$-k_1$	$+k_3$	k_s	Pump-probe (k_1)
$+k_2$	$-k_2$	$+k_3$	k_s	Pump-probe (k_2)
$+k_1$	$+k_2$	$-k_3$	k_s	Double Quantum
$+k_1$	$+k_1$	$-k_3$	k_s	Double Quantum
$+k_2$	$+k_2$	$-k_3$	k_s	Double Quantum
$+k_2$	$+k_1$	$-k_3$	k_s	Double Quantum

2.3 Focus size measurements

The focusing of the mid-IR light in the sample plane was measured by scanning a 5-μm-diameter pinhole in the X and Y directions at the focus plane and recording the integrated intensity of the transmitted light at the MCT array. The slit at the input of the spectrometer was fully opened in order to suppress optical distortions produced by imaging the pinhole into the spectrometer input. Similarly, a 25-μm-diameter pinhole was used to measure the focus size of the FTIR light with a single-channel MCT detector. Frequencies between 1960 and 2060 cm^{-1} were used to calculate the FTIR focus size.

2.4 Sample preparation

For the purposes of illustrating the capabilities of this microscope, nonlinear IR spectroscopy was performed on the CO stretching vibrations of metal carbonyls, which were incorporated into polystyrene beads to create a heterogeneous sample environment. Polystyrene beads (d = 100–125 μm, Polysciences Inc.) were swelled in a 17 mM $Mn_2(CO)_{10}$ (Sigma-Aldrich) in chloroform solution for a period of one hour, washed with methanol and dried under mild vacuum for approximately two hours before use. The final concentration of $Mn_2(CO)_{10}$ in the polymer matrix is estimated to be 1.8 mM based on the IR absorption of a bead. Samples

#213680 - $15.00 USD Received 13 Jun 2014; revised 16 Jul 2014; accepted 16 Jul 2014; published 25 Jul 2014

were stored dry in a dark environment between uses. Bead samples were held between two 1-mm CaF_2 windows in the 2D IR microscope.

3. Results

3.1 Point spread function

Figure 3(a) shows the transmission of the probe focus (E_3) through a 5-μm pinhole. A two-dimensional Gaussian fit to the intensity plot yields a full width at half-maximum of 12.2 μm and 18.6 μm along the X and Y axes, respectively. The theoretical diffraction limit for our 0.45 NA objective is 4.4 μm (FWHM). The Rayleigh range of the focus in the direction of propagation, measured using a razor edge, is approximately 90 μm. For comparison, the focus size of FTIR at 1960–2060 cm^{-1} [Fig. 3(b)] is 96.8 μm x 79.7 μm along the X and Y dimensions, nearly an order of magnitude larger compared with the 2D IR input. This simple comparison illustrates the improvement in resolution associated with using coherent, well-collimated light for microscopy. Analogous to two-photon fluorescence microscopy, the nonlinear signal depends on the square of the intensity; this way the resolution is further improved, possibly to below the diffraction limit.

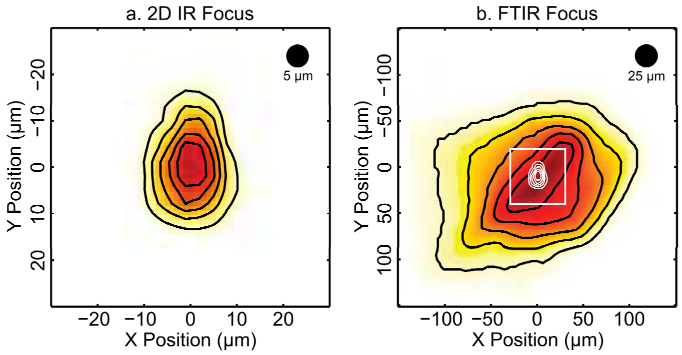

Fig. 3. Microscope point spread function (PSF) at the focus plane in transmission mode. (a) PSF of well-collimated IR output from the OPA/DFG setup used for 2D IR. (b) PSF measured internal thermal source from FTIR. The plots were obtained by scanning a 5- and 25-μm pinhole in the focus plane, respectively. Note the different plot scales; contours from (a) are also included in (b) for comparison.

The brightness of our well-collimated mid-IR source is approximately $3x10^{20}$ photons/(s $mrad^2$ 0.1%BW), considerably higher compared with an FTIR thermal source (1500 K) which is $1x10^{15}$ photons/(s $mrad^2$ 0.1%BW @ 5 μm), and even higher than synchrotron sources such as the Diamond Light Source [$5x10^{16}$ photons/(s $mrad^2$ 0.1%BW @5 μm)] [24]. The above comparisons indicate IR imaging would likely benefit from high-brightness, femtosecond IR sources, albeit at the expense of limited spectral bandwidth, though tunable throughout the mid-IR. Two important caveats are worth considering: *1.* signal-to-noise ratios are often limited by the shot-to-shot noise and laser instabilities instead of detector noise, and *2.* the duty time of the experiments is much lower compared with CW sources. It is also important to mention that the high electric field intensities (~10^{13} W/cm^2, an upper limit for the experiments presented here) that arise from a tightly focusing short laser pulses can easily generate multiphoton signals in the sample or windows, or ultimately damage the sample.

3.2 Two-dimensional infrared microspectroscopy (2DIMS)

Figure 4 shows a bright field image of a 100-μm polystyrene bead with $Mn_2(CO)_{10}$ embedded into the polystyrene matrix. 2D IR spectra are measured at each spatial position indicated by the grid; a sample 2D IR spectrum is displayed on the right pane. Peaks appear as positive/negative doublets along the detection axis due to vibrational anharmonicity. The

#213680 - $15.00 USD Received 13 Jun 2014; revised 16 Jul 2014; accepted 16 Jul 2014; published 25 Jul 2014

2008 cm^{-1} diagonal peak, corresponding to the equatorial C≡O stretching mode [25] is mapped onto the color scale. The map correlates well to the optical path of the bead; the signal is most intense near the center of the bead where the optical path is longest, and decays toward the edges of the bead. Evidently, the spherical shape of the bead induces lensing effects at the focus, as seen in the inhomogeneity in the signal amplitude inside the bead region. Three main diagonal peaks centered near 1979, 2008, and 2045 cm^{-1}, along with the corresponding cross peaks are observed in the spectrum. The low-frequency diagonal peak, along with its corresponding cross peaks are weak compared with $Mn_2(CO)_{10}$ in cyclohexane. This attenuation, however, is due to a small absorption band of polystyrene centered around 1940 cm^{-1} (OD ~0.2 at bead center) that extends into the low frequency range of the $Mn_2(CO)_{10}$ spectral window. As expected, the line shapes are qualitatively similar to those measured in nonpolar solvents [26]. These proof-of-principle experiments demonstrate 2DIMS for spatially resolved spectroscopic mapping in heterogeneous samples.

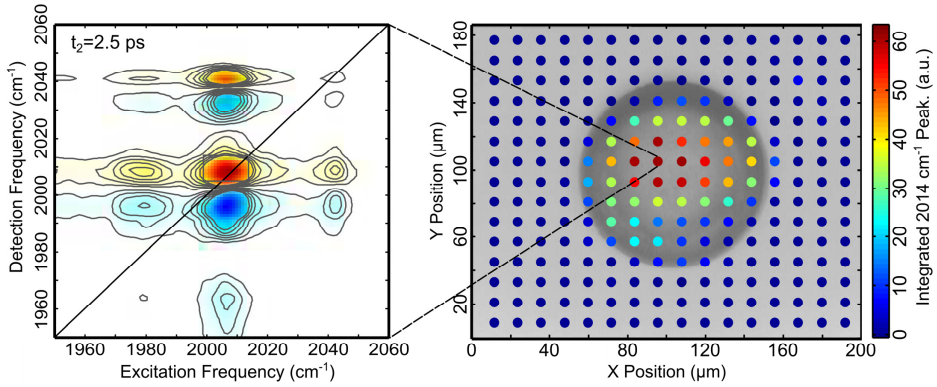

Fig. 4. (right) 2D IR chemical map of a 100-μm-diameter polystyrene bead with $Mn_2(CO)_{10}$. The color bar represents the integrated intensity of the diagonal 2008 cm^{-1} peak in the 2D IR spectrum as indicated by a box in the right plot. The points are overlaid onto a brightfield visible image of the bead. (left) Absorptive 2D IR spectrum of $Mn_2(CO)_{10}$ collected at the position indicated in the image. A total data acquisition time of 100 seconds is required for each 2D IR spectrum, corresponding to each point in the image map to the left. The total data acquisition time for the complete map is 6 hours and 15 minutes.

3.3 Stimulated-emission lifetime IR microscopy (SLIM)

To take advantage of the high time resolution and dynamical information afforded by ultrafast IR spectroscopy, and inspired by fluorescence lifetime imaging microscopy (FLIM), a method widely used for biological imaging [27, 28], we demonstrate the use of vibrational lifetime as a contrast agent for spatial mapping of heterogeneous chemical (solvation) environments. The rate of vibrational energy relaxation of a chromophore reports on the local solute–solvent interactions, serving as the contrast agent for imaging heterogeneous environments, such as solvent polarity or viscosity distributions. The main difference between infrared and fluorescence imaging is that nonradiative vibrational relaxation occurs on shorter time scales (~1–200 ps) compared with spontaneous emission (~1–100 ns), so an IR probe pulse stimulates emission—and induces further absorption to higher excited states—at a specific delay following the pump pulse. While we refer to this technique as a vibrational *lifetime* microscopy, two other mechanisms contribute to decay of the signal: intramolecular vibrational redistribution (IVR) and diffusive orientational relaxation. Regardless of the particular decay mechanism, the key advantage of this method is that measurements remain independent of concentration as the map contrast originates exclusively from the probe–solvent interactions, reporting on the local solvent environment.

#213680 - $15.00 USD Received 13 Jun 2014; revised 16 Jul 2014; accepted 16 Jul 2014; published 25 Jul 2014

Figure 5 shows the pump–probe signal decay of $Mn_2(CO)_{10}$ as a function of delay between pump and probe in the polystyrene bead and in methanol. Polystyrene is a weakly interacting solvent, whereas methanol hydrogen bonds to the carbonyl oxygens, enhancing the rate of vibrational energy relaxation, thus causing the signal decay rate to virtually double as a function of waiting time in methanol. These measurements are carried out using transient absorption—or pump–probe—spectroscopy in place of 2D IR since the data acquisition time required for pump–probe spectra is considerably shorter compared with 2D IR and the information of interest, namely the waiting time dependence of the signal, is easily extracted from pump–probe measurements.

Measuring the full signal decay at each spatial point requires extended data acquisition times, therefore we measure the pump–probe signal amplitude at two delays: 5 ps and 100 ps, using the ratio of these two points as a proxy for the decay rate. Figure 5 (right) shows a spatial map of the signal amplitude ratio represented by the color of the dots at specific X,Y positions around a polystyrene bead. The $Mn_2(CO)_{10}$ containing bead is prepared similar to the bead for chemical imaging above, but in place of air the bead is surrounded by a solution of $Mn_2(CO)_{10}$ in methanol.

Areas of fast relaxation appear in blue and slower decays in red. Slower relaxation rates are observed inside the bead compared with the surrounding solvent. Points surrounding the bead edge appear red. We suspect that this is because the finite three-dimensional shape of the bead acts as a lens, bending the IR light toward the center of the bead. The raw pump–probe signal intensity (not shown) near the edge of the bead is approximately an order of magnitude lower compared with the center of the bead, thus causing the lifetime measurement to have a higher uncertainty near the interface. Total data acquisition time at each point is 30 seconds. The data illustrates the use of SLIM to map heterogeneous environments using a single reporter species.

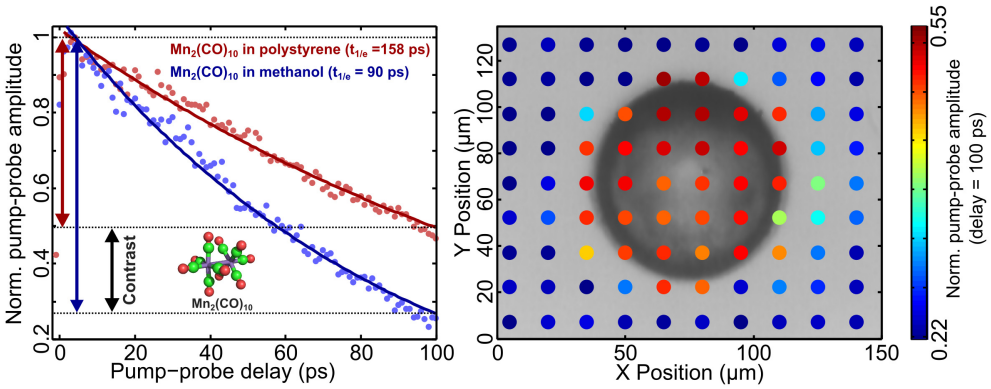

Fig. 5. (left) Pump–probe signal intensity plot as a function of delay between pump and probe for $Mn_2(CO)_{10}$ in a polystyrene bead (red) and methanol (blue). The solid curves represent single-exponential fits to the data. (right) Vibrational lifetime map of $Mn_2(CO)_{10}$ in a polystyrene bead and surrounding methanol solvent. The color bar represents the pump–probe amplitude of the 2008 cm^{-1} peak at 100 ps following excitation.

4. Discussion

4.1 Collinear 2D IR geometry

The collinear geometry has advantages and drawbacks compared with the pump–probe or boxcars geometries. One beam offers a simplified alignment of the IR throughout the optical setup, and the phase-stability is critical for heterodyne-detected nonlinear techniques such as 2D IR. Pulses travel along the same path and undergo identical phase changes at each interface, and thus remain phase locked with respect to each other and the signal. Spectra remain robust with respect to changes in alignment and sample heterogeneity. The new geometry opens up new possibilities for measuring nonlinear spectra in heterogeneous

#213680 - $15.00 USD Received 13 Jun 2014; revised 16 Jul 2014; accepted 16 Jul 2014; published 25 Jul 2014

environments on the micron length scale. While not specific to the collinear geometry, it is worth mentioning that the phase-cycling ability of the shaper can be used to further separate the rephasing and nonrephasing signals to extract additional information from the measurements [29]. In practice, one important requirement for obtaining high-quality spectra is high shot-to-shot pulse stability. Interference terms (Table 1) are nearly an order of magnitude larger than the nonlinear signal, and while the phase-cycling cancelation is, in principle, complete, the eight-frame cycle demands that the pulse intensity remain stable between shots.

It is also worth mentioning that we have successfully collected 2D IR spectra in transflection mode using the microscope setup described above. A sample was prepared by depositing a ~2 mM solution of $Mn_2(CO)_{10}$ in squalane on top of a gold surface and covering it with a 1-mm CaF_2 window using a 50-μm spacer. As shown in Fig. 2, the light enters and exits through the objective. Transflection mode, however, attenuates the IR by a factor of approximately four, producing a lower 2D IR signal compared with transmission mode. The 2D IR spectrum collected in transflection mode [Fig. 6] looks virtually identical to spectra collected in transmission mode (not shown).

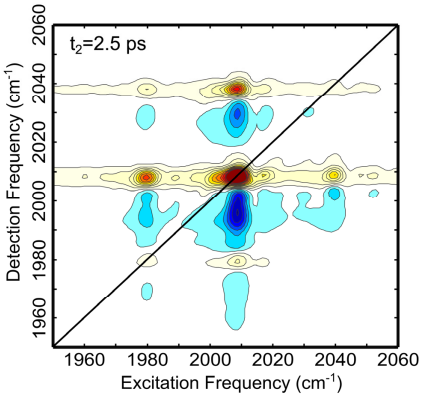

Fig. 6. 2D IR spectrum of $Mn_2(CO)_{10}$ in squalane solution collected in transflection mode in the IR microscope using the fully collinear beam geometry.

4.2 Assessment of 2D IR microspectroscopy

In general, vibrational imaging based on IR or Raman spectroscopy has great appeal as a label-free *in situ* probe of molecular phenomena. These methods have growing impact in many areas of biology and medicine [15, 30], and are widely used in the analysis of heterogeneous materials including polymers, coatings, pharmaceuticals, and fibers. Both methods provide chemical sensitivity through intrinsic vibrational resonances, but in other ways differ. In comparison with IR absorption microscopy, Raman microscopy offers the high spatial resolution afforded by the visible wavelengths and higher transparency for *in vitro* studies and biological imaging. IR is influenced less than Raman in imaging turbid or scattering media and offers a complementary range of transparency. Nonlinear Raman methods, such as coherent anti-Stokes Raman scattering (CARS) and stimulated Raman scattering (SRS) microscopy, greatly improve sensitivity compared with spontaneous Raman, have achieved video-rate imaging speeds, and have the narrower point spread function of nonlinear optical microscopies [31–33].

In comparison to existing IR and Raman microscopies such as those above, 2D IR spectroscopy adds extra levels of molecular sensitivity to structure and dynamics in spatially resolved measurements. Current methods map spatially varying chemical composition in terms of the spatial concentration variations of chemical functional groups at a selected resonance frequency. In complex heterogeneous media, a number of ambiguities can arise. For instance, multiple molecular species can be resonant at a given frequency. Similarly,

#213680 - $15.00 USD Received 13 Jun 2014; revised 16 Jul 2014; accepted 16 Jul 2014; published 25 Jul 2014

since the spatial resolution is still macroscopic, the overlap of two different chemical species in an IR or Raman image does not mean that these species are molecularly associated. Structurally, 2D IR reveals vibrational correlations through cross peaks that can be used to uniquely separate multiple species in a congested spectrum and to demonstrate the absence or presence of molecular scale contacts between species. Its dynamical sensitivity means that such correlations can be revealed with the assistance of dynamical phenomena such as vibrational energy transfer, spectral diffusion, orientational dynamics, or chemical exchange.

Although there are clear applications to imaging, in the short term we envision that the value of the nonlinear IR microscopy methods presented here will be for localized spectroscopy within a spatially heterogeneous sample. At present, 2D IR microscopy cannot achieve the spatial resolution or fast imaging rates that are common in nonlinear Raman or fluorescence microscopy. However, it offers multiple frequency and time dimensions that can be used to spectrally or temporally dissect a complex vibrational spectrum at selected points in space. 2D IR microspectroscopy provides the capability of separating heterogeneous samples in space, time, and frequency, with a real space resolution of microns, but Ångstrom-scale molecular resolution. Its femtosecond temporal resolution means that 2D IR microscopy can be used to extract molecule- or bond-specific dynamics in order to understand how molecular dynamics are affected by local environments.

There are additional benefits that arise from the tight focusing and high brightness of our IR source. Focus spots are small enough to that one can perform spectroscopy on single cells, characterize the composition and spatial distributions of molecules within many eukaryotic cells, and use in conjunction with microfluidic devices. Its high brightness means that one can perform structurally sensitive spectroscopy on challenging samples such as protein microcrystals, propagate further in highly absorbing media, and study subwavelength samples and optics. In addition, coherent IR sources could be beneficial for high-throughput linear or nonlinear spectral imaging using focal plane arrays. Of course, the high peak intensities ($\sim 10^{12\text{-}13}$ W/cm^2) of ultrafast IR sources is also a notable disadvantage for bioimaging, although average power is low (~1 mW).

4. Summary and outlook

We described a new fully collinear optical geometry for nonlinear mid-IR microspectroscopy. The geometry enabled us to measure spectra with nearly diffraction-limited spatial resolution in a commercial IR microscope, opening new avenues for measuring spatially resolved 2D IR and pump–probe spectra. In addition to spatial resolution, the high peak intensities at the nearly diffraction-limited focus, increase the nonlinear signal intensities, allowing for increased sensitivity, and shorter data acquisition times. We have also demonstrated the use of vibrational lifetime as a concentration-independent contrast agent for a single IR chromophore in heterogeneous chemical environments.

In overall perspective, 2D IR microscopy offers unique capabilities to measure spatially resolved chemical structure and dynamics, opening up the possibilities for *in situ* nonlinear mapping of heterogeneous materials and biological samples with micron-length spatial resolution. We expect that continued advancement of optical technologies will result in data acquisition times comparable to FTIR spectra. The methods described here have great potential for measuring real-time molecular dynamics without the need for fluorescent labels or stains.

Acknowledgments

The project was supported by the National Science Foundation (CHE-1212557 and CHE-1414486) as well as from a startup grant from the University of Chicago. C. Baiz gratefully acknowledges fellowship support from a National Institutes of Health (NIH) Ruth L. Kirschstein National Research Service Award (F32GM105104). D. Schach thanks the Deutsche Forschungsgemeinschaft (DFG) for a research fellowship (SCHA 1816/1).

#213680 - $15.00 USD Received 13 Jun 2014; revised 16 Jul 2014; accepted 16 Jul 2014; published 25 Jul 2014